

# Ferroionic inversion of spin polarization in a spin-memristor

Cite as: APL Mater. 9, 031110 (2021); <https://doi.org/10.1063/5.0039030>

Submitted: 29 November 2020 . Accepted: 05 March 2021 . Published Online: 23 March 2021

 V. Rouco,  F. Gallego,  D. Hernandez-Martin,  D. Sanchez-Manzano, J. Tornos, J. I. Beltran, M. Cabero,  F. Cuellar, D. Arias,  G. Sanchez-Santolino, F. J. Mompean, M. Garcia-Hernandez, A. Rivera-Calzada, M. Varela, M. C. Muñoz,  C. Leon,  Z. Sefrioui, and  J. Santamaria

## COLLECTIONS

Paper published as part of the special topic on [Magnetoelectric Materials, Phenomena, and Devices](#)



View Online



Export Citation



CrossMark

## ARTICLES YOU MAY BE INTERESTED IN

[Strain-gradient effects in nanoscale-engineered magnetoelectric materials](#)

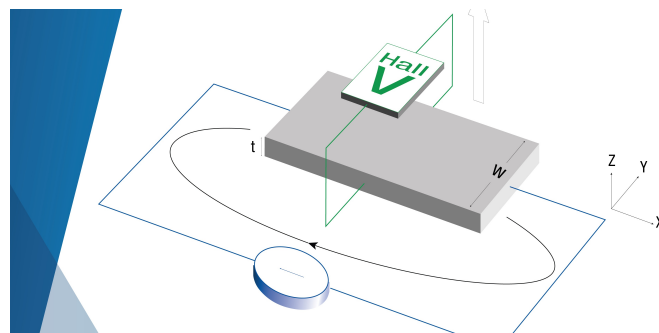
APL Materials **9**, 020903 (2021); <https://doi.org/10.1063/5.0037421>

[A new era in ferroelectrics](#)

APL Materials **8**, 120902 (2020); <https://doi.org/10.1063/5.0034914>

[Pyroelectric thin films—Past, present, and future](#)

APL Materials **9**, 010702 (2021); <https://doi.org/10.1063/5.0035735>



**Tips for minimizing  
Hall measurement errors**

Download the Technical Note



# Ferroionic inversion of spin polarization in a spin-memristor

Cite as: APL Mater. 9, 031110 (2021); doi: 10.1063/5.0039030

Submitted: 29 November 2020 • Accepted: 5 March 2021 •

Published Online: 23 March 2021



View Online



Export Citation



CrossMark

V. Rouco,<sup>1</sup> F. Gallego,<sup>1,2</sup> D. Hernandez-Martin,<sup>1</sup> D. Sanchez-Manzano,<sup>1</sup> J. Tornos,<sup>1</sup> J. I. Beltran,<sup>1,3</sup> M. Cabero,<sup>4</sup> F. Cuellar,<sup>1</sup> D. Arias,<sup>1,a)</sup> G. Sanchez-Santolino,<sup>1,3</sup> F. J. Mompean,<sup>2,5</sup> M. Garcia-Hernandez,<sup>2,5</sup> A. Rivera-Calzada,<sup>1,5</sup> M. Varela,<sup>1,3</sup> M. C. Muñoz,<sup>5,6</sup> C. Leon,<sup>1,5</sup> Z. Sefrioui,<sup>1,5</sup> and J. Santamaria<sup>1,5,b)</sup>

## AFFILIATIONS

<sup>1</sup>GFMC, Universidad Complutense de Madrid, 28040 Madrid, Spain

<sup>2</sup>2D-Foundry Group, Instituto de Ciencia de Materiales de Madrid ICMM-CSIC, 28049 Madrid, Spain

<sup>3</sup>Instituto Pluridisciplinar, Universidad Complutense de Madrid, 28040 Madrid, Spain

<sup>4</sup>Centro Nacional de Microscopia Electronica, Universidad Complutense, 28040 Madrid, Spain

<sup>5</sup>Unidad Asociada UCM/CSIC, "Laboratorio de Heteroestructuras con Aplicación en Spintrónica", 28040 Madrid, Spain

<sup>6</sup>Instituto de Ciencia de Materiales de Madrid ICMM-CSIC, 28049 Madrid, Spain

**Note:** This paper is part of the Special Topic on Magnetoelectric Materials, Phenomena, and Devices.

<sup>a)</sup>**On leave from:** Universidad del Quindío. Armenia. Colombia.

<sup>b)</sup>**Author to whom correspondence should be addressed:** [jacsan@ucm.es](mailto:jacsan@ucm.es)

## ABSTRACT

Magnetoelectric coupling in artificial multiferroic interfaces can be drastically affected by the switching of oxygen vacancies and by the inversion of the ferroelectric polarization. Disentangling both effects is of major importance toward exploiting these effects in practical spintronic or spinorbitronic devices. We report on the independent control of ferroelectric and oxygen vacancy switching in multiferroic tunnel junctions with a  $\text{La}_{0.7}\text{Sr}_{0.3}\text{MnO}_3$  bottom electrode, a  $\text{BaTiO}_3$  ferroelectric barrier, and a Ni top electrode. We show that the concurrence of interface oxidation and ferroelectric switching allows for the controlled inversion of the interface spin polarization. Moreover, we show the possibility of a spin-memristor where the controlled oxidation of the interface allows for a continuum of memresistance states in the tunneling magnetoresistance. These results signal interesting new avenues toward neuromorphic devices where, as in practical neurons, the electronic response is controlled by electrochemical degrees of freedom.

© 2021 Author(s). All article content, except where otherwise noted, is licensed under a Creative Commons Attribution (CC BY) license (<http://creativecommons.org/licenses/by/4.0/>). <https://doi.org/10.1063/5.0039030>

The incorporation of ferroic materials in electronic devices is a strategy being pursued to reduce their power consumption. The recent proposal of the novel magnetoelectric spin orbit logic device based on the use of multiferroic materials to control magnetization<sup>1,2</sup> has boosted the interest in magnetoelectric devices for spintronics and spinorbitronics.<sup>3</sup> Magnetoelectric coupling exists naturally in multiferroics, but it can be achieved also in artificial interfaces combining ferroelectric and ferromagnetic materials. This is the case of the so-called multiferroic tunnel junctions, which are tunnel devices with ferromagnetic electrodes and a ferroelectric barrier. In these devices, the inversion of the ferroelectric polarization produces large changes in the value of the tunneling conductance giving rise to the tunneling electroresistance.<sup>4–16</sup> This effect is driven

by the modulation of the height of the tunnel barrier by the direction of the ferroelectric polarization.<sup>4,5</sup> Besides tunneling conductance, the direction of the ferroelectric polarization also produces large modifications of the spin polarization of the interface<sup>15,17,18</sup> through its effect on hybridization and bonding<sup>19–22</sup> and/or spin dependent screening.<sup>23,24</sup> This is an interesting magnetoelectric effect that could be the source of novel device concepts.

Another family of interesting phenomena in multiferroic tunnel junctions comes from the switching of oxygen vacancies, which modifies the oxidation of interfaces. Early works in the field of oxide tunnel junctions have also outlined the role played by oxidation of the interface in modifying its spin polarization. It has been shown that different oxide barriers have different bonding and

hybridization with the orbitals of the ferromagnet yielding different exchange splitting of bonding and antibonding orbitals and accordingly different spin polarization of the interface bands.<sup>25,26</sup> Oxide devices typically involve interfaces between ultrathin oxide layers where oxygen vacancies are usually present and can be driven by the strong electric fields building up in these devices.<sup>27</sup> Their accumulation at interfaces, besides modifying conductance in resistive switching processes, has been shown to change their magnetic state enabling the electric field control of magnetism in magnetoionic devices.<sup>28–32</sup>

Multiferroic tunnel junctions, thus, may present effects related to the inversion of the ferroelectric polarization and to the switching of oxygen vacancies both yielding changes in the tunneling conductance and in the magnetoelectric response.<sup>33</sup> Moreover, both the electrochemical and the ferroelectric states of the interface may couple in what has been called ferroionic states where the stability of the ferroelectric polarization is controlled by the electrochemistry of surfaces and interfaces.<sup>34</sup> The relative importance of both effects on magnetoelectric coupling has been the subject of debate and controversy. Disentangling the effect of oxygen vacancy and ferroelectric switching is a major step to harness magnetoelectric coupling in multiferroic tunnel junctions toward its future applications in spintronics and spinorbitronics.

In this paper, we show the possibility of separately controlling ferroelectric and oxygen vacancy switching on the same device. We show that the concurrence of interface oxidation and ferroelectric switching allows for the controlled inversion of the interface spin polarization. We moreover show the possibility of a spin-memristor where the controlled oxidation of the interface allows for a continuum of memristance states in the tunneling magnetoresistance.

We have used a high pressure (3.4 mbar) pure oxygen sputtering technique to epitaxially grow BaTiO<sub>3</sub> (BTO)/La<sub>0.7</sub>Sr<sub>0.3</sub>MnO<sub>3</sub> (LSMO) bilayers onto (001) SrTiO<sub>3</sub> (STO) substrates. This technique has been shown to produce atomically sharp LSMO/BTO interfaces as demonstrated by scanning transmission electron microscopy (STEM) high angle annular dark field (HAADF) imaging combined with atomic column resolution electron energy-loss spectroscopy (EELS) elemental maps.<sup>35,36</sup> Piezo-force microscopy demonstrated ferroelectric switching in these bilayers and the ability to write and erase domains.<sup>35</sup>

La<sub>0.7</sub>Sr<sub>0.3</sub>MnO<sub>3</sub> (25 nm)/BaTiO<sub>3</sub> (4 nm)/Ni (20–50 nm) multiferroic tunnel junctions fabricated on micrometer-size pillars are defined by combined optical lithography techniques and ion milling. Electroresistance was measured in the temperature range of 20–100 K by recording the low voltage (10 mV) resistance after applying (for ~100 ms) dc voltages varied in a hysteresis loop sequence. The results are shown in Fig. 1(a). Positive (negative) voltages in Fig. 1 correspond to electric fields pointing up (down).

We observe quite asymmetric counterclockwise electroresistance loops with sharp resistance switches at large voltages of  $\pm 4$  V (hereafter major loops). A low resistance state (LRS) is achieved at large ( $-4$  V) negative voltages, which switches into an intermediate resistance state (IRS) at 4 V. Once in the IRS, reducing voltage yields an additional gradual switch starting at  $-1$  V into a high resistance state (HRS) that switches back into the LRS at  $-4$  V. Counterclockwise major loops thus have positive electroresistance [ER = (R(V) – R(–V))/R(–V)]. If the sense of the voltage sweep is reversed from the HRS, minor electroresistance loops have been found connecting

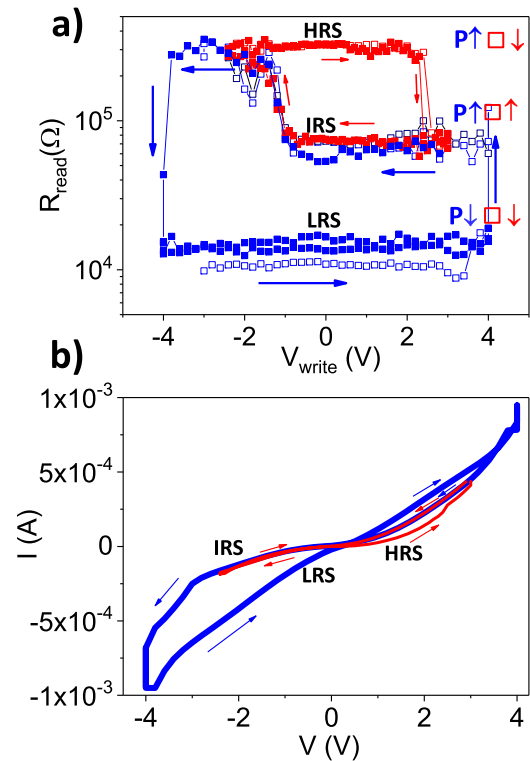


**FIG. 1.** Ferroelectric and oxygen vacancy resistance dc loops. (a) Electroresistance loops (10 mV) of a Ni/BTO/LSMO multiferroic tunnel junction measured at 30 K. The different resistance states are identified according to the orientation up (P $\uparrow$ ) or down (P $\downarrow$ ) of the ferroelectric polarization and to the location up ( $\square\uparrow$ ) or down ( $\square\downarrow$ ) of oxygen vacancies (i.e., oxygen vacancies pushed by electric field against to the top or the bottom BTO interface). (b) IV loops illustrating the switching between the three resistance states. Wide voltage loops (in blue) show the switching of the ferroelectric polarization and oxygen vacancies. Narrow voltage range loops show the switching of the oxygen vacancies only.

the HRS and the IRS with somewhat reduced values of the coercive electric fields ( $-1.5$  and  $2.5$  V). Note that minor loops are clockwise (negative electroresistance) reflecting that different processes underlie both switching loops. Non-linear IV curves characteristic of tunneling transport were obtained. Voltage loops measuring IV curves [see Fig. 1(b)] capture the three resistance states shown by electroresistance loops.

The counterclockwise major loops (with sharp switches at coercivity) are driven by the inversion of the ferroelectric polarization. Note that the high resistance state attained at positive voltages corresponds to polarization-up state for which the high resistance state is expected according to the giant electroresistance model,<sup>5</sup> where the hole doping at LSMO to screen the negative polarization charges in the P-up state triggers an increase in the average height of the tunneling barrier. On the other hand, the gradual flank at negative voltages indicates that minor loops are triggered by the switching of oxygen vacancies, which exist naturally in these ultrathin oxide layers, as inferred from combined high resolution electron microscopy together with energy-loss electron spectroscopy showing reduced Ti oxidation states (3.85–3.90) at the surface. The switching of oxygen

vacancies is a slow process as compared with the switching of the ferroelectric polarization, which occurs in the range of hundreds of picoseconds to a few nanoseconds.<sup>37</sup> The switching of oxygen vacancies on the other hand is known to produce electric field relaxation in impedance spectroscopy experiments limited by their ionization and transport, which yield characteristic times in the audio frequency range.

We have examined the evolution of the minor loops with voltage pulse excitation of a duration ranged between 100 ns and 10 ms. While pulses are long enough to switch ferroelectric polarization, the relaxation time of the oxygen vacancy switch is expected to be precisely in this range. Single pulses have been applied with different amplitudes following hysteresis loops. IV curves in the voltage range of  $-1$  to  $1$  V have been measured between pulses to quantify resistance from the  $dV/dI$  derivative at  $750$  mV [see Fig. 2]. In actual measurements, the LSMO bottom electrode was grounded, which preserved the better square pulse shape; however, voltage in the x axis of Fig. 2 has been mirrored to allow direct comparison with the measurements of Fig. 1. We can qualitatively compare pulse measurements ( $50$  K) and dc measurements ( $30$  K) since, being in the tunneling regime, the resistance displays a weak dependence on temperature (see Fig. S1 of the supplementary material). Note that the pulse excitations yielded negative electroresistance and resemble the minor loops at large ( $>1$  ms) pulse duration, albeit with a larger positive voltage coercive field. However, the amplitude of the loops decreases when the duration of the pulse is reduced toward the  $100$  ns level, and it remains stable in the value corresponding to the HRS for the shortest pulses. This shows that the minor loop drives oxygen vacancies between the bottom (LSMO/BTO) and the top (Ni/BTO) interfaces and that the stable configuration is oxygen vacancies accumulating toward the top interface, i.e., in positive voltages, oxygen vacancies switch with ferroelectric polarization although cycling of the electric field can be used to switch them to

accumulate at the bottom interface yielding the HRS. Experiments of pulse switching at different temperatures showed that longer pulses are necessary to switch oxygen vacancies when the temperature is lower, indicating that the process is thermally activated.

The reason for the asymmetry in the major electroresistance loop thus becomes clear. It results from the concurrent switching of ferroelectric polarization and oxygen vacancies at the positive coercive field at  $4$  V from the LRS with polarization down and oxygen vacancies down ( $P\downarrow, \square\downarrow$ ) to the IRS state with polarization pointing up and oxygen vacancies pushed toward the top interface ( $P\uparrow, \square\uparrow$ ). The reduced resistance compared to the HRS ( $P\uparrow, \square\downarrow$ ) results from the opposite effects of ferroelectric polarization, which increases resistance and oxygen vacancy switching that lowers it.

The finding of three resistance states (instead of the four, one could expect from the independent switching of oxygen vacancies and the ferroelectric polarization) demonstrates the ferroionic coupling of oxygen vacancies and of the ferroelectric polarization. While in the polarization-down state ferroelectricity and oxygen vacancies switch concurrently, their switching is decoupled in the polarization-up state to form the more stable HRS (note the difference in the switching fields) with oxygen vacancies accumulating at the bottom interface.

A very interesting consequence is that since both the LRS ( $P\downarrow, \square\downarrow$ ) and the HRS ( $P\uparrow, \square\downarrow$ ) have oxygen vacancies accumulating at the bottom interface, the resistance change between the LRS and HRS is entirely caused by the switching of the ferroelectric polarization through its effect on the barrier height<sup>5</sup> and/or the electronic structure of the interfaces, i.e., this rules out that resistance switching is due to the formation of filaments, which would be driven by different oxygen vacancy states. Spontaneous (massive) oxidation of the Ni electrode can also be discarded since it would render a high resistance state for both orientations of the ferroelectric polarization.

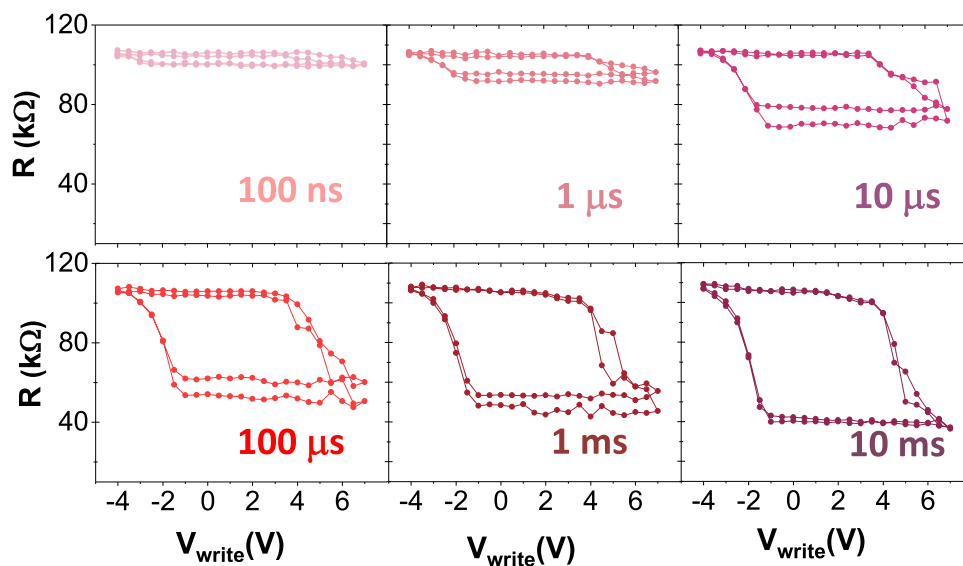


**FIG. 2.** Resistance loops of oxygen vacancies measured with voltage pulse excitation. Differential resistance as a function of pulse amplitude at  $50$  K after applying pulses with different amplitude (V) and time width. Several loops are shown for each pulse duration to assess stability never surpassing  $-4$  V to avoid ferroelectric switching.

Such a process would be energetically disfavored by the highly negative formation Gibbs free energy of  $\text{TiO}_2$  ( $-884.5$  kJ/mol) compared with that of  $\text{NiO}$  ( $-211.7$  kJ/mol).<sup>38</sup> It appears that the  $\square\downarrow$  oxygen vacancy state produces a subtle oxidation of the Ni interface whose electronic states are modulated by the ferroelectric switching.

Next, we describe the magnetoresistance response of our devices. We measured electrical transport of the multiferroic tunnel junctions in magnetic fields applied along the  $[110]$  direction (easy axis of LSMO). Tunnel magneto-resistance [ $\text{TMR} = (R_{\text{AP}} - R_{\text{P}})/R_{\text{P}}$ ] was computed from magnetic field ( $H$ ) sweeps where resistance [ $R(H)$ ] was recorded as a function of field.  $R(H)$  curves (see Fig. 3) showed abrupt switches allowing to identify parallel and antiparallel alignment of LSMO and Ni layer moments. Magnetoresistance was also obtained from  $I(V)$  curves acquired in the parallel ( $R_{\text{P}}$ ) and antiparallel (or misaligned) ( $R_{\text{AP}}$ ) magnetic configurations. First, TMR was measured after applying electric fields to select either the low resistance (LRS) or the high resistance (HRS) electroresistance states. Positive TMR was obtained in the LRS ( $\text{P}\downarrow, \square\downarrow$ ), while the HRS ( $\text{P}\uparrow, \square\downarrow$ ) produced negative TMR, as shown in Figs. 3(a) and 3(b). By switching resistance in the oxygen vacancy loop and making use of the gradual low voltage flank, resistance could be stabilized at different memresistance states [see Fig. 3(c)] between the IRS and the HRS identified in Fig. 3(d). Different memresistance states had also different TMR [see Fig. 3(e)], thus displaying

a spin-memrestive behavior. TMR was strongly reduced toward the IRS ( $\text{P}\uparrow, \square\uparrow$ ). Since LSMO is a half metal with positive spin polarization, the positive TMR indicates also a positive spin polarization of the top interface. LSMO based ferroelectric tunnel junctions with polarization pointing up have shown large positive TMR, indicating positive spin polarization.<sup>36</sup> The negative TMR in the HRS thus indicates an inversion of the spin polarization of the top interface driven by the inversion of ferroelectric polarization (note that both the LRS and HRS are in the same  $\square\downarrow$  state concerning the oxygen vacancies). The strong reduction of the TMR when the IRS is approached upon switching oxygen vacancies from the HRS to the IRS is thus connected to the oxidation of the top Ni/BTO interface. On the other hand, the first TMR switch in the HRS occurs at positive magnetic fields (before crossing zero field) and with much larger coercivity than the LRS indicating substantial changes of magnetic anisotropy, which forces magnetic moments to point away from the  $[110]$  field direction. The bias dependence of the MR in both the LRS and HRS is also markedly different. While the positive TMR in the LRS is weakly dependent on bias [see Fig. 3(a)], the negative TMR of the HRS is strongly bias dependent and is suppressed by bias voltages of 100 mV [see Fig. 3(b)], which indicates that the tunneling process giving rise to the negative TMR is driven by a highly localized electronic state close to the Fermi energy. This localized state probably results from the interface bonding of interfacial oxygen to Ni

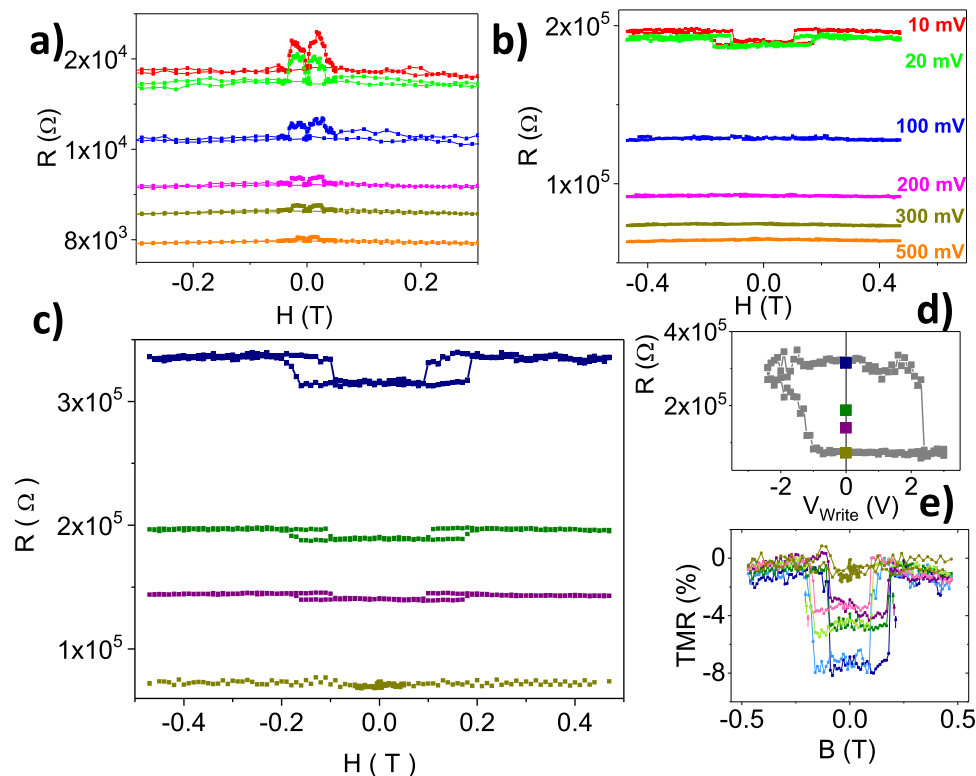


**FIG. 3.** Ferroionic control of the tunneling magnetoresistance (TMR). TMR at 15 K at different bias voltages measured in the LRS (a) and in the HRS (b). (c) TMR measured at 10 mV at different resistance states as indicated in (d) between the HRS and the IRS. (e) Detail of the TMR switches. Note that the first TMR switch occurs before crossing zero field. A low temperature (15 K) was chosen to prevent samples for shorts during the many cycles necessary to show the TMR of the different resistance states. However, TMR depends only weakly in the temperature range of 15–100 K (see Fig. S2 of the [supplementary material](#)).

that assists the tunneling process giving rise to a resonant inversion of the spin polarization as described previously.<sup>39</sup> Furthermore, an atomically thin NIO layer at the interface in contact with the Ni has been shown, along with the inversion of the spin polarization, to develop canted moments, which drive deep changes of magnetic anisotropy.<sup>40</sup>

It is important to remark that, although interface oxidation is at the bottom of the observed behavior, the inversion of the spin polarization is driven by ferroelectric switching, and it is not a pure magnetoionic effect as observed recently in hafnia based multiferroic junctions.<sup>41</sup> On the other hand, multilevel control of TMR by the domain state of the ferroelectric has been shown in Co/PZT/LSMO structures,<sup>18</sup> but in this case, it results from the controlled switching of oxygen vacancies in a way determined by the orientation of the ferroelectric polarization, i.e., not only oxidation or ferroelectric switching but also their concurrence determines the observed inversion of the spin polarization and the observed spin memristor effect. We speculate that ferroelectricity, through its effect on hybridization, may have a drastic effect on the electronic structure (and consequently magnetic anisotropy) of the interface as shown recently for the Fe/BTO interface where the inversion of the ferroelectric polarization triggers the transition between interfacial ferromagnetic and antiferromagnetic states.<sup>42</sup> Further studies will be directed to clarify the effect of polarization on the electronic structure of the Ni BTO interface.

In summary, we have found that the controlled independent switching of ferroelectric polarization and oxygen vacancies in multiferroic tunnel junctions shows the presence of electronic states controlled by the interplay between ferroelectric and electrochemical processes. The gradual switching of oxygen vacancies in the presence of a definite polarization state has allowed the observation of a continuum of spin memristive states. These results signal interesting new avenues toward neuromorphic devices where, as in practical neurons, the electronic response is controlled by electrochemical degrees of freedom.

See the [supplementary material](#) for Figs. S1 and S2.

The authors acknowledge funding received from the project Quantox of QuantERA ERA-NET Cofund in Quantum Technologies (Grant Agreement No. 731473) implemented within the European Union's Horizon 2020 Programme. This work was supported by Spanish MINECO through Grant No. MAT2017-87134-C02. V.R. acknowledges the European Union's Horizon 2020 research and innovation programme (Marie Skłodowska-Curie IF Grant Agreement No. OXWALD 838693) and the Spanish Ministry of Science, Innovation and Universities through a Juan de la Cierva Incorporación fellowship (Grant No. IJC2018-035192-I). G.S.-S. acknowledges the financial support from Spanish MICIU (Grant Nos. RTI2018-099054-J-I00 and MICINN IJC2018-038164-I).

## DATA AVAILABILITY

The data that support the findings of this study are available from the corresponding author upon reasonable request.

## REFERENCES

- <sup>1</sup>S. Manipatruni, D. E. Nikonov, and I. A. Young, *Nat. Phys.* **14**, 338 (2018).
- <sup>2</sup>S. Manipatruni *et al.*, *Nature* **565**, 35 (2019).
- <sup>3</sup>P. Noël *et al.*, *Nature* **580**, 483 (2020).
- <sup>4</sup>J. P. Velev, C.-G. Duan, J. D. Burton, A. Smogunov, M. K. Niranjan, E. Tosatti, S. S. Jaswal, and E. Y. Tsymlal, *Nano Lett.* **9**, 427 (2009).
- <sup>5</sup>M. Y. Zhuravlev, R. F. Sabirianov, S. S. Jaswal, and E. Y. Tsymlal, *Phys. Rev. Lett.* **94**, 246802 (2005).
- <sup>6</sup>V. Garcia, S. Fusil, K. Bouzehouane, S. Enouz-Vedrenne, N. D. Mathur, A. Barthélémy, and M. Bibes, *Nature* **460**, 81 (2009).
- <sup>7</sup>P. Maksymovych, S. Jesse, P. Yu, R. Ramesh, A. P. Baddorf, and S. V. Kalinin, *Science* **324**, 1421 (2009).
- <sup>8</sup>A. Gruverman, D. Wu, H. Lu, Y. Wang, H. W. Jang, C. M. Folkman, M. Y. Zhuravlev, D. Felker, M. Rzchowski, C.-B. Eom, and E. Y. Tsymlal, *Nano Lett.* **9**, 3539 (2009).
- <sup>9</sup>D. Pantel, S. Goetze, D. Hesse, and M. Alexe, *ACS Nano* **5**, 6032 (2011).
- <sup>10</sup>D. Pantel, H. Lu, S. Goetze, P. Werner, D. Jik Kim, A. Gruverman, D. Hesse, and M. Alexe, *Appl. Phys. Lett.* **100**, 232902 (2012).
- <sup>11</sup>D. Pantel, S. Goetze, D. Hesse, and M. Alexe, *Nat. Mater.* **11**, 289 (2012).
- <sup>12</sup>L. Jiang, W. S. Choi, H. Jeon, S. Dong, Y. Kim, M.-G. Han, Y. Zhu, S. V. Kalinin, E. Dagotto, T. Egami, and H. N. Lee, *Nano Lett.* **13**, 5837 (2013).
- <sup>13</sup>Z. Wen, C. Li, D. Wu, A. Li, and N. Ming, *Nat. Mater.* **12**, 617 (2013).
- <sup>14</sup>X. Liu, J. D. Burton, and E. Y. Tsymlal, *Phys. Rev. Lett.* **116**, 197602 (2016).
- <sup>15</sup>Q. H. Qin, L. Äkäslompolo, N. Tuomisto, L. Yao, S. Majumdar, J. Vijayakumar, A. Casiraghi, S. Inkinen, B. Chen, A. Zugarramurdi, M. Puska, and S. van Dijken, *Adv. Mater.* **28**, 6852 (2016).
- <sup>16</sup>J. Li, N. Li, C. Ge, H. Huang, Y. Sun, P. Gao, M. He, C. Wang, G. Yang, and K. Jin, *iScience* **16**, 368 (2019).
- <sup>17</sup>V. Garcia, M. Bibes, L. Bocher, S. Valencia, F. Kronast, A. Crassous, X. Moya, S. Enouz-Vedrenne, A. Gloter, D. Imhoff, C. Deranlot, N. D. Mathur, S. Fusil, K. Bouzehouane, and A. Barthelemy, *Science* **327**, 1106 (2010).
- <sup>18</sup>Z.-D. Luo, G. Apachitei, M.-M. Yang, J. J. P. Peters, A. M. Sanchez, and M. Alexe, *Appl. Phys. Lett.* **112**, 102905 (2018).
- <sup>19</sup>C.-G. Duan, S. S. Jaswal, and E. Y. Tsymlal, *Phys. Rev. Lett.* **97**(4), 047201 (2006).
- <sup>20</sup>M. Fechner *et al.*, *Phys. Rev. B* **78**, 212406 (2008).
- <sup>21</sup>M. Fechner, S. Ostanin, and I. Mertig, *Phys. Rev. B* **80**, 094405 (2009).
- <sup>22</sup>S. Valencia *et al.*, *Nat. Mater.* **10**(10), 753–758 (2011).
- <sup>23</sup>J. D. Burton and E. Y. Tsymlal, *Phys. Rev. B* **80**(17), 174406 (2009).
- <sup>24</sup>M. Y. Zhuravlev, S. Maekawa, and E. Y. Tsymlal, *Phys. Rev. B* **81**, 104419 (2010).
- <sup>25</sup>J. M. De Teresa *et al.*, *Science* **286**, 507 (1999).
- <sup>26</sup>E. Y. Tsymlal, I. I. Oleinik, and D. G. Pettifor, *J. Appl. Phys.* **87**, 5230 (2000).
- <sup>27</sup>S. V. Kalinin and N. A. Spaldin, *Science* **341**, 858 (2013).
- <sup>28</sup>U. Bauer *et al.*, *Nat. Mater.* **14**, 174–181 (2014).
- <sup>29</sup>C. Bi *et al.*, *Phys. Rev. Lett.* **113**, 267202 (2014).
- <sup>30</sup>H.-B. Li *et al.*, *Nat. Commun.* **8**, 2156 (2017).
- <sup>31</sup>D. Gilbert *et al.*, *Nat. Commun.* **7**, 11050 (2016).
- <sup>32</sup>C. Leighton, *Nat. Mater.* **18**, 13 (2019).
- <sup>33</sup>H. Kohlstedt, A. Petraru, K. Szot, A. Rüdiger, P. Meuffels, H. Haselier, R. Waser, and V. Nagarajan, *Appl. Phys. Lett.* **92**, 062907 (2008).
- <sup>34</sup>S. M. Yang, A. N. Morozovska, R. Kumar, E. A. Eliseev, Y. Cao, L. Mazet, N. Balke, S. Jesse, R. K. Vasudevan, C. Dubourdieu, and S. V. Kalinin, *Nat. Phys.* **13**, 812 (2017).
- <sup>35</sup>G. Sanchez-Santolino *et al.*, *Nat. Nanotechnol.* **12**, 655 (2017).
- <sup>36</sup>J. Tornos *et al.*, *Phys. Rev. Lett.* **122**, 037601 (2019).
- <sup>37</sup>E. Parsonnet *et al.*, *Phys. Rev. Lett.* **125**, 067601 (2020).
- <sup>38</sup>D. D. Wagman *et al.*, *J. Phys. Chem. Ref. Data* **11**(Suppl. 2), 166 (1982).
- <sup>39</sup>E. Y. Tsymlal, A. Sokolov, I. F. Sabirianov, and B. Doudin, *Phys. Rev. Lett.* **90**, 186602 (2003).
- <sup>40</sup>H. Yang, S.-H. Yang, D.-C. Qi, A. Rusydi, H. Kawai, M. Saeys, L. Titus, D. J. Smith, and S. P. P. Parkin, *Phys. Rev. Lett.* **106**, 167201 (2011).
- <sup>41</sup>Y. Wei, S. Matzen, C. P. Quinteros, T. Maroutian, G. Agnus, P. Lecoeur, and B. Noheda, *npj Quantum Mater.* **4**, 62 (2019).
- <sup>42</sup>G. Radaelli *et al.*, *Nat. Commun.* **5**, 3404 (2014).